International Journal of Energy, Environment, and Economics ISSN: 1054-853X
Volume 25, Issue 2

TRANSIENT STUDY OF A HEAT MANAGEMENT SYSTEM: APPLICATION TO THE MYRTE PLATFORM

Dalia Si Ahmed[1,*], Nadia Bendjaballah-Lalaoui[2], Manuel Espinosa-López[1] and Christian Cristofari[1]

[1]Laboratory Science for the Environment UMR 6134,
University of Corsica Pasquale Paoli, Ajaccio, France
[2]Laboratory of Catalytic Materials and Catalysis in Organic Chemistry,
University of Science and Technology Houari Boumediene, Algiers, Algeria

ABSTRACT

Renewable energies have emerged as an alternative to fossil fuels, following the increase of energy consumption, greenhouse gas emissions, electricity peak demands and energy costs. The MYRTE platform is a large-scale demonstrator that produces and stores electricity using photovoltaic and hydrogen. The platform includes PEM fuel cell and electrolyzer units that can achieve temperatures of about 70°C and has the potential to simultaneously provide electrical and thermal power for various applications. This cogeneration can improve the efficiency of the hydrogen chain by allowing the heat produced by these units to be stored for reuse in a secondary network (for example, the heating circuit of a building). The aim of the present paper is to study the transient behavior of a heat management system that manages thermal recovery and storage for the cooling of the fuel cell and electrolyzer units. This system is composed of a 14 m^3 glycol-water storage tank surrounded by a mantle heat exchanger able to store 800 kWh day^{-1}, a dry cooler, a process heat exchanger and a heat exchanger dedicated to recovery applications. To estimate the temperatures and the powers involved, we model–the various components of the heat management system using energy balance equations. We solve the obtained model with Matlab Simulink, and the results show that the simulation accurately predicts the measured parameters with a maximum temperature deviation of 2 °C. The stratification of the storage tank is also studied and compared with an equivalent mean temperature method. The temperatures obtained from these two methods are found to agree within a nRMSE of 6%.

Keywords: Heat management, thermal management, cogeneration, waste heat, heat recovery, MYRTE platform.

* Corresponding Author's E-mail: si-ahmed_d@univ-corse.fr

NOMENCLATURE

Symbols		**Acronyms**	
A	Heat exchange area [m^2]	AC	Alternating Current
Cp	Specific heat [J kg^{-1} K^{-1}]	DC	Direct Current
d	Diameter [m]	PEM	Proton Exchange Membrane
$\boldsymbol{\Delta T_{mean}}$	Mean arithmetic temperature [K]	PID	Proportional–Integral–Derivative controller
$\boldsymbol{\Delta T_{lm}}$	Logarithmic mean temperature difference [K]	**Greek**	
$\boldsymbol{\Delta x_i}$	Distance between two nodes [m]	ε	Thickness [m]
h	Convective heat transfer coefficient [W m^{-2} K^{-1}]	ρ	Density [kg m^{-3}]
k	Thermal conductivity [W m^{-1} K^{-1}]	η	Efficiency (thermal/electrical) [-]
KQ	Flowmeter	**Subscripts**	
KT	Heat sensor	0	Initial time
PO	Pump	amb	Ambient
L	Length or Height [m]	Al	Aluminium
M	Mass [kg]	cooler	Dry cooler
$\boldsymbol{\dot{m}}$	Mass flow rate [kg s^{-1}]	gw	Glycol-water
$\boldsymbol{\dot{Q}}$	Cooling/heating power [W]	hex	Heat exchanger
R	Universal gas constant [8.31 J $mol^{-1}K^{-1}$]	in	Inlet
$\mathbf{R_{th}}$	Thermal resistance [m^2 K W^{-1}]	inox	Stainless steel
t	Time [s]	insul	Insulation
T	Temperature [°C]	man	Mantle heat exchanger
U	Overall heat transfer coefficient [W m^{-2} K^{-1}]	out	Outlet
V	Volume [m^3]	pipe	Pipeline
$\boldsymbol{\dot{W}}$	Electric power [W]		

1. INTRODUCTION

The International Energy Agency (IEA) has collected data on trends in energy consumption. Over the last four decades (1973 to 2014), the world primary energy consumption has increased by 224% and CO_2 emissions by 209%, with an average annual increase of nearly 5.1% [1]. Since the beginning of the last century, the global average temperature has increased by about 0.6°C according to the United Nations (UN) Intergovernmental Panel on Climate Change (IPCC). According to a 2001 report [3], the temperature can still increase from 1.4 to 4.5°C until 2100 [2]. Mean global temperatures as calculated by a linear trend show a warming of 0.85°C (0.65 to 1.06 °C) over the period 1880-2012.

According to this critical situation, the international community decided to take initiatives to stop the overall temperature increase process. One of these initiatives is the Kyoto Protocol, a legally binding agreement that took place in 1997 whereby industrialized countries would reduce their collective greenhouse gas emissions by 5.2% between 2008 and 2012, in order to go back to gas emission levels comparable to those of 1990. This reduction specifically targets carbon dioxide, which is the inevitable by-product of industrial activities. To achieve this goal, industries should improve facilities and processes [2].

In 2014, the European Union signed a historic agreement on its climate plan, with a reduction of at least 40% in greenhouse gas emissions by 2030, and pledged to increase its

share of renewable energies to 27% of consumption [4]. In 2015, the United Nations Climate Change Conference (COP 21) was held in France gathering 196 nations from around the world. The conference gave rise to the Paris agreement to avoid climate changes [5]. The Protocol commits the signatories to willingly consider holding the increase in the global average temperature to 2°C above pre-industrial levels and reducing greenhouse emissions to carbon neutrality.

Over the past few years, there has been an intensification of research aimed at developing technologies that offer reductions in energy consumption, peaks in electricity demand and energy costs, while maintaining constant level comfort conditions [6]. In this quest to find an alternative to fossil fuels, renewable energies have become a global focal point.

The interest in countries benefiting from a large solar field for the use of solar-powered technologies has grown. This clean, abundant energy not only provides electricity, but also heating, drying and cooking [8].

In this context, the MYRTE platform emerged as a collaboration between the University of Corsica Pasquale Paoli, the industrial partner Areva Energy Storage and the Commission for Atomic Energy and Alternative Energy (CEA). The platform shown in Figure 1 was inaugurated in 2012 in Ajaccio, Corsica (south of France). This platform was meant to upgrade the power grid by restoring the electrical photovoltaic power stored thanks to a hydrogen chain [9].

The aim of the present paper is to investigate numerically the MYRTE platform heat management system in order to quantify heat recovery, and as a result enhance the overall platform performance and fulfill cogeneration. The paper is divided into four main sections. Section 1 introduces the context of this study, namely the platform MYRTE. In Section 2, the material and methods are developed along with the modelling steps, and the dynamic simulation of the heat management system is detailed. In Section 3, the obtained results are discussed, while the main important outputs are summarized in Section 4.

Figure 1. View on the platform MYRTE (Ajaccio, Corsica).

1.1. Context of the Study - MYRTE Platform

The MYRTE platform which covers nearly one hectare is composed of several subsystems as illustrated in Figure 2.

1. **A field of photovoltaic panels**
   The PV field comprises 2240 monocrystalline panels tilted at 30°, for a total surface area of 3700 m² and a maximum power of 560 kWp. 28 inverters allow the conversion of the direct current of the photovoltaic energy into alternating current.
2. **A unit of electrolyzers**
   The stack of the PEM (Proton Exchange Membrane) water electrolyzer is composed of 60 cells of 280 cm² active area, with a rated power of 46 kW DC. The nominal gas production rates are 10 $Nm^3\ h^{-1}$ of H_2 and 5 $Nm^3\ h^{-1}$ of O_2; its maximum operating pressure is 35 bar.
3. **A fuel cell Unit**
   The PEM fuel cell subsystem of MYRTE has a net generating capacity of about 100 kW electric AC. Its core is a network of 4 stacks mounted in electrical series and supplied in parallel fluid. Each stack contains 100 cells of active surface area per cell equal to 400 cm². The nominal electric power produced by each stack is 25 kW DC.
4. **Storage tanks of O_2 and H_2**
   The storage consists of a gaseous O_2 storage tank, as well as two gaseous H_2 storage tanks with a volume of 28 m^3 each (1400 Nm^3 of H_2 and 700 Nm^3 of O_2). The gases are stored at a pressure of 10 to 35 bar.
5. **A heat management system**
   The heat management process allows the temperature control of the electrolysis and fuel cell subsystems in order to comply with the optimum operating temperatures of 60°C and 70 °C, without exceeding the maximum operating temperature of 75°C. For this purpose, the system must ensure the availability of coolant at a maximum temperature of 45°C (set point temperature) when returning to the fuel cell [10].
6. **Tools of control and electrical conversion**
   The control-command subsystem of the MYRTE platform forms the core of the operation of the entire plant. It controls all the subsystems and defines the instructions for each of them, depending on the application concerned: peak shaving, photovoltaic power production guaranteed or PV production smoothing.
7. **A GreEnergy box**
   In 2013, a subsystem composed of a 50 kW PEM fuel cell and a 60 kW PEM electrolyzer is added to strengthen the platform. The heat produced by this box is released to the atmosphere.

During periods of low energy consumption and on a sunny day, the electrical energy produced by photovoltaic panels is directed towards the electrolyzer, which will carry out a separation of water into two circuits of hydrogen and oxygen gases; they will be stored in high storage tanks.

In the event of an increase in consumption and in the absence of sunshine, the reverse operation takes place. The fuel cell restores the electric energy stored by consuming both

gases and producing heat. Then, this energy will be injected into the electrical grid. The consumption peak shaving mode aims at limiting the use of thermal power plants and at overcoming the limit of 30% for integrating intermittent renewable energy imposed by the French Commission for the Regulation of Energy in 2008 [12].

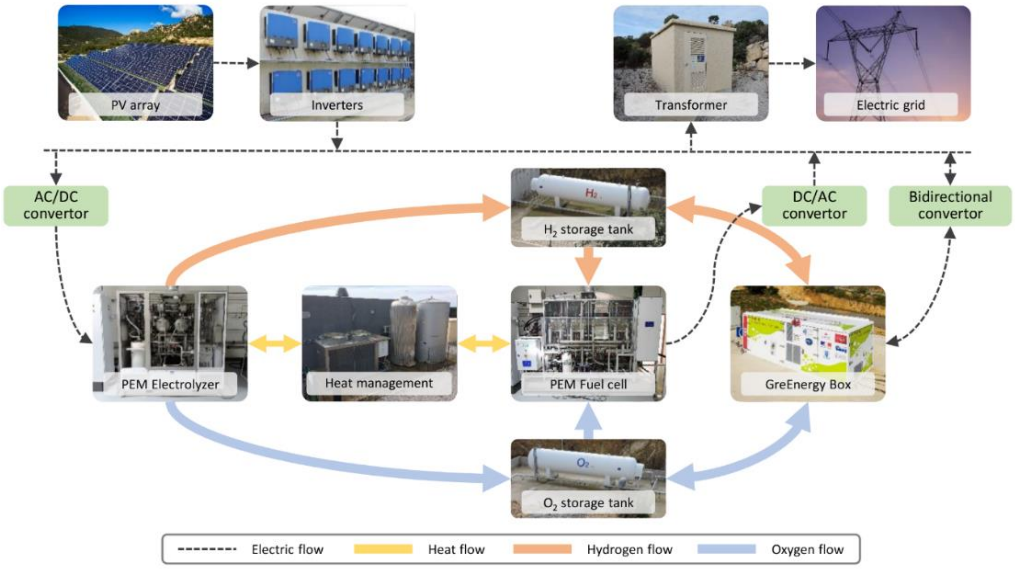

Figure 2. Subsystems of the platform MYRTE [11].

1.2. Cogeneration

The heat produced by the fuel cell and the electrolyzer can be upgraded by supplying hot water to adjacent buildings, by heating them or even produce cold for a tri-generation system [13].

The platform has the capacity to deliver thermal power at a temperature up to 70°C, which limits the options for the recovery of the heat produced into a cogeneration system. Table 1 shows some of these potential applications, and the conditions under which they can be achieved. Thermally activated energy generators such as organic Rankine cycles, Stirling engines and steam turbines are excluded because they require higher temperatures than those provided by the fuel cell.

Table 1. Cogeneration of MYRTE with technologies thermally activated

Applications	Technologies	Temperature (°C)	Auxiliary Heat
Heating	Heated floor	~ 19 – 29	Exempted
	Sanitary hot water	~ 50 – 60	Recommended
Cooling	Absorption chillers	~ 120	Needed
	Adsorption chillers	~ 55	Recommended
Humidity control	Sorption desiccation	~ 25	Exempted
Bio-fuels	Bio-digesters	~ 30 – 55	Exempted

For technologies requiring an average operating temperature around 50°C, backup heating is recommended to overcome temperature variations at the heat management system output that strongly depend on the operation mode of the platform (clipping, smoothing... etc.).

1.3. Heat Management System

The recovery and storage modes of the heat management system allow the cooling of the electrolyzer and fuel cell units. It enables the heat produced by these units to be stored for reuse in a secondary network. This system includes a dry cooler, a recovery heat exchanger, a mantle heat exchanger, and a heat storage of 14 m^3 able to store up to 800 kWh day^{-1}. The system operates according to four functional modes as shown in Figure 3.

1.3.1. Cooling Mode with Storage and Dry Cooler

If the storage is not full, the hot fluid coming from the main process heat exchanger goes through the recovery heat exchanger before transferring its calories to the storage tank by mean of the mantle heat exchanger. The fluid is then directed, thanks to the pump PO500, toward the dry cooler where its temperature decreases until reaching the set point temperature fixed by the control-command subsystem.

1.3.2. Cooling Mode without Storage and Dry Cooler

This mode occurs if the storage is full, or if the return temperature of the water from the fuel cell and electrolyzer is lower than the set point. In this state, the mantle heat exchanger is isolated, and the fluid is directly diverted to the dry cooler.

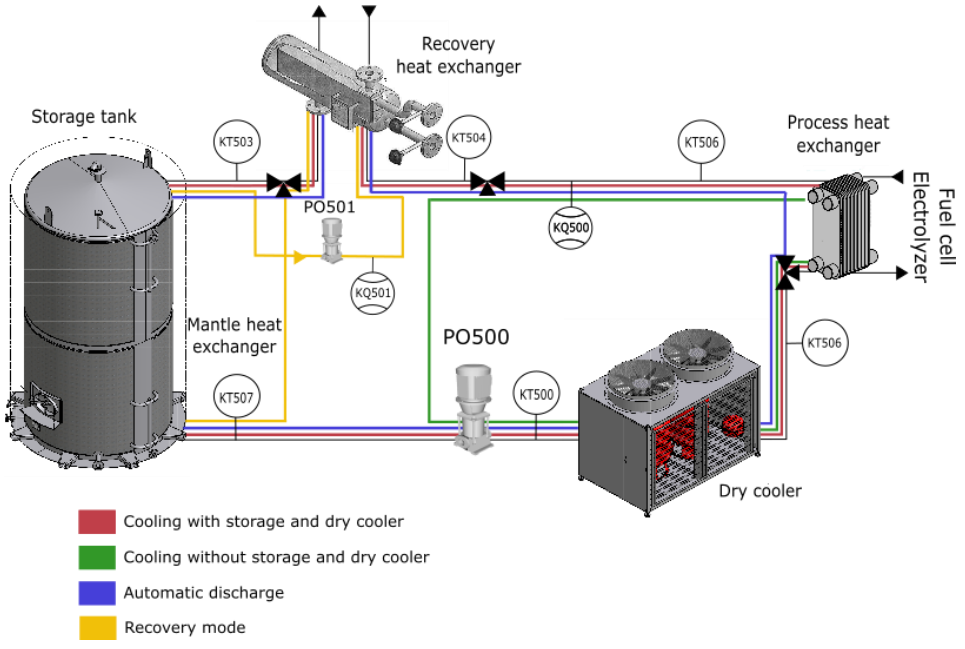

Figure 3. Representative diagram of the SSCHA [14].

1.3.3. Automatic Discharge without Heat Recovery

The system allows the removal of heat previously stored by using the dry cooler and the storage tank without passing through the main process heat exchanger. In this state, the system is autonomous, and the fluid is governed by the closure of a 3-way valve located at the entrance of the process heat exchanger.

1.3.4. Heat Recovery Mode

If the cooling mode is no longer required, this mode allows recovering the thermal energy stored in the storage tank through the recovery heat exchanger. To investigate the potential of the stored heat to furnish hot water for various applications.

When the storage is full, which means that the tank has reached its maximum temperature and it absorbs no more heat from the system, the heat stored in the tank can be extracted for recovery purposes. To fulfill the heat recovery mode, the mantle heat exchanger, the tank, and the recovery heat exchanger are isolated by swiveling the motorized 3-way valves. The rest of the excess heat of the fuel cell and electrolyzer is directed toward the dry cooler until the end of the recovery mode. At the same time, in a second circuit, the second pump (PO501) extracts the fluid from the upper part of the mantle exchanger instead of the lower part as in the classical operation mode. The fluid goes through the recovery heat exchanger where it transfers its heat to a third fluid circuit, supplying a cogeneration system.

2. MATERIALS AND METHODS

2.1. Mathematical Modeling

To depict the thermal behavior inside the process, the energy balance equation for each element is established using the lumped thermal equivalent capacitance. The developed model presents separately the various elements considered: heat exchangers, tank, pumps and pipelines. The first order differential equation for each element of the system is used to calculate the temperature of the fluid coming out of the compartment (T_{out}). This temperature is supposed to be equal to the mean temperature of the considered control volume (liquid, metal, and insulation material). The physical properties within the system such as volume, pressure, density, and specific heat are assumed to be constant and independent of temperature.

2.1.1. Process Heat Exchanger

The temperature of the fluid leaving the process heat exchanger is calculated from the heat produced by the fuel cell and electrolyzer units as shown in Eq. (1):

$$T_{process,out} = T_{process,in} + \frac{\dot{Q}_{process}}{\dot{m}_{gw} \cdot c_{p,gw}} \quad (1)$$

2.1.2. Recovery Heat Exchanger

The cold fluid to be heated circulates inside the plates of the heat exchanger while the hot glycol-water circulates inside the shell. The exchanger is made of stainless steel and is

covered with an insulation material (expanded polystyrene). The model used for the recovery heat exchanger is given below:

Shell (hot side)

$$\left(M_{gw}c_{p,gw} + M_{inox}c_{p,inox} + M_{insul}c_{p,insul}\right)_{shell}\frac{dT_{shell,out}}{dt} = \dot{m}_{gw}c_{p,gw}\left(T_{shell,in} - T_{shell,out}\right) - (U\cdot A)_{hex}\,\Delta T_{lm} - (U\cdot A)_{shell}\left(T_{shell,mean} - T_{amb}\right) \quad (2)$$

The right-hand side of Eq. (2) includes the energy of the circulating hot fluid, the heat exchanged with the cold side, and the thermal loss to the outside. The arithmetic mean temperature of the shell is calculated using Eq. (3).

$$T_{shell,mean} = (T_{shell,in} + T_{shell,out})/2 \quad (3)$$

Plates (cold side)

$$\left(M_{gw}c_{p,gw} + M_{Al}\,c_{p,Al}\right)_{plates}\frac{dT_{plates,out}}{dt} = -\dot{m}_{wg}c_{p,gw}\left(T_{plates,out} - T_{plates,in}\right) + (U\cdot A)_{hex}\cdot\Delta T_{lm} \quad (4)$$

The right-hand side of Eq. (4) represents the energy of the circulating cold fluid and the heat exchanged with the hot side. The global thermal transfer coefficient of the shell with the ambient is obtained by considering the various elements defining its structure, namely: the hot fluid convection, the conduction inside the metal, the conduction through the insulation material-and the air convection-as formulated in Eq. (5).

$$(U\cdot A)_{shell} = \left(\frac{1}{R_{th}}\right)_{shell} = 1\Big/\left(\frac{1}{h_{gw}A_{shell}} + \frac{ln\left(\frac{R_{shell}+\varepsilon_{inox}}{R_{shell}}\right)}{(2\pi L_{shell})k_{inox}} + \frac{ln\left(\frac{R_{shell}+\varepsilon_{inox}+\varepsilon_{insul}}{R_{shell}+\varepsilon_{inox}}\right)}{(2\pi L_{shell})k_{insul}} + \frac{1}{h_{air}\,A_{insul}}\right) \quad (5)$$

The heat exchanged between the hot and the cold side of the recovery heat exchanger is calculated using the overall surface heat transfer coefficient:

$$(U\cdot A)_{hex} = \left(\frac{1}{R_{th}}\right)_{hex} = 1\Big/\left(\frac{1}{h_{gw}A_{exchange}} + \frac{\varepsilon_{inox}}{k_{inox}\,A_{exchange}} + \frac{1}{h_{gw}\,A_{exchange}}\right) \quad (6)$$

The mean logarithmic temperature ΔT_{lm} for the two counter-current circulating fluids is giving as follows:

$$\Delta T_{lm} = \frac{\Delta T_1 - \Delta T_2}{ln(\Delta T_1/\Delta T_2)} = \frac{(T_{shelll,in} - T_{plates,out}) - (T_{shell,out} - T_{plates,in})}{ln[(T_{shell,in} - T_{plates,out})/(T_{shell,out} - T_{plates,in})]} \quad (7)$$

If there is no convergence of the numerical solution of the differential equation for the temperature, and if the temperature range on one side of the exchanger does not exceed 50% of the temperature range on the other side of the exchanger, we may substitute the arithmetic mean ΔT_{mean} for ΔT_{lm}. The error would then be less than 1%.

$$\Delta T_{mean} = ((T_{shell,in} - T_{plates,out}) - (T_{shell,out} - T_{plates,in}))/2 \quad (8)$$

2.1.3. Dry Cooler

The electrical cooling device is composed of a pump, two fan coils and 500 m of tubes and fins, as shown in Figure 4. The dry cooler can be considered as a glycol-water/air heat exchanger. To calculate the temperature of the glycol-water leaving the cooler, the thermal inertia of the hot liquid and the metallic tube are considered in Eq. (9). The right-hand side of the equation involves the glycol-water heat flow inside the tubes and the heat exchanged with the surrounding air [15].

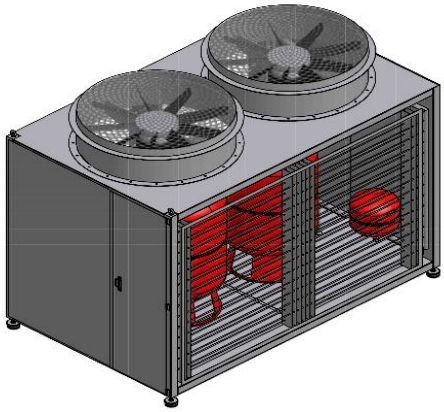

Figure 4. Representative diagram of the dry cooler [14].

$$\left(M_{gw}c_{p,gw} + M_{Al}c_{p,Al}\right)_{cooler} \frac{dT_{cooler,out}}{dt} = \dot{m}_{gw}c_{p,gw}\left(T_{cooler,in} - T_{cooler,out}\right) - (U \cdot A)_{cooler}\left(T_{cooler,mean} - T_{amb}\right) \quad (9)$$

The dry cooler is operated with a PID (proportional–integral–derivative) controller. The fan coils are activated if the measured fluid temperature exceeds the set point temperature. If the first proportional fan is not sufficient to dissipate the heat, the second fan that operates in all-or-none principle is triggered.

2.1.4. Circulation Pump

The temperature of the glycol-water leaving the circulation pump is calculated thanks to the electrical and thermal power of the pump in Eq. (10) [15].

$$T_{pump,out} = T_{pump,in} + \frac{\dot{Q}_{thermal}}{\dot{m}_{gw} \cdot c_{p,gw}} \quad (10)$$

where $\dot{Q}_{thermal}$ is the thermal energy of the pump transferred to the fluid. This parameter was evaluated by using the electrical power of the pump $\dot{W}_{electric}$ and the pump efficiency η_{pump}.

$$\dot{Q}_{thermal} = (1 - \eta_{pump}) \cdot \dot{W}_{electric} \quad (11)$$

2.1.5. Pipelines

The heat management system is linked with approximately 20 m of inox pipelines, half of which is non-insulated. To calculate the temperature of the fluid leaving the pipeline, the following equation is considered:

$$\left(M_{gw}c_{p,gw} + M_{inox}c_{p,inox} + M_{insul}c_{p,insul}\right)_{pipe}\frac{dT_{pipe,out}}{dt} = \dot{m}_{gw}c_{p,gw}\left(T_{pipe,in} - T_{pipe,out}\right) - (U\cdot A)_{pipe}\left(T_{pipe,mean} - T_{amb}\right) \quad (12)$$

The thermal resistance of the pipeline toward the fluid heat loss to the ambient includes the glycol-water convection, the conduction through the metal, the conduction of the insulation material and the air convection-as shown in Eq. (13):

$$(U\cdot A)_{pipe} = \left(\frac{1}{R_{th}}\right)_{pipe} = \frac{1}{\frac{1}{h_{gw}(2\pi R_1)} + \frac{ln\left(\frac{R_2}{R_1}\right)}{(2\pi L_{pipe})k_{inox}} + \frac{ln\left(\frac{R_3}{R_2}\right)}{(2\pi L_{pipe})k_{insul}} + \frac{1}{h_{air}(2\pi R_3)}} \quad (13)$$

where R_1, R_2 and R_3 are the inner radius of the pipe, the outer radius and the radius with insulation, respectively.

2.1.6. Mantle Heat Exchanger and Storage Tank

The 14 m^3 storage tank is surrounded by a thin mantle heat exchanger that contains the hot glycol-water coming from the recovery heat exchanger. To determine the temperatures at the hot and the cold side, two methods are employed: the first method is based on an equivalent mean temperature for the whole volume [16], the second one investigates the thermal stratification of the two equipments.

Method 1: Equivalent Mean Temperature

Storage tank (cold side)

At the cold side, we consider the following equation:

$$\left(M_{gw}c_{p,gw} + M_{inox}c_{p,inox}\right)_{tank}\frac{dT_{tank,mean}}{dt} = (U\cdot A)_{man-tank}\left(T_{tank,mean} - T_{man,mean}\right) - (U\cdot A)_{tank}\left(T_{tank,mean} - T_{amb}\right) \quad (14)$$

The left-hand side of the equation defines the thermal inertia of the tank and its contents, while the right-hand side includes the energy of the hot glycol-water inside the mantle along with the loss to the ambient at both top and bottom of the tank.

Mantle (hot side)

$$\left(M_{gw}c_{p,gw} + M_{inox}c_{p,inox} + M_{insul}c_{p,insul}\right)_{man}.\frac{dT_{man,out}}{dt} = -\dot{m}_{gw}\,c_{p,gw}\,(T_{man,in} - T_{man,out}) - (U.A)_{man}\left(T_{man,mean} - T_{amb}\right) \quad (15)$$

The right-hand side of the equation represents the energy of the hot glycol-water given to the storage tank and the thermal energy lost to the outside. The thermal resistance of the mantle heat exchanger is calculated using Eq. (16), which considers the hot fluid convection, the conduction of the metallic wall and the cold fluid convection. The exchange coefficient with the ambient air is calculated as for the pipeline.

$$(U \cdot A)_{man-tank} = \left(\frac{1}{R_{th}}\right)_{man-tank} = \frac{1}{\frac{1}{h_{gw} A_{man}} + \frac{ln\left(\frac{R_{tank}+\varepsilon_{inox}}{R_{tank}}\right)}{(2\pi L_{tank}) k_{inox}} + \frac{1}{h_{gw} A_{tank}}} \quad (16)$$

Method 2: Thermal Stratification

Thermal stratification is a phenomenon that occurs most often in liquids and air. Stratification is caused by a natural distribution of temperatures where the low density hot liquid floats at the top of the reservoir and the cooler liquid of higher density stays downward, with intermediate temperature layers between these two areas.

Nowadays, there are various modeling approaches for studying the stratification of surface heat exchange tanks, depending on whether the fluid flow is considered uni-, bi-, or multi-dimensional [17]. A two-dimensional implicit Finite Differences Method is considered for the calculation of the temperature inside the mantle heat exchanger and the storage tank. These two compartments are split in 8 sections (8 nodes) with energy balance characterizing each section of these compartments (Figure 5). The choice of the number of nodes is based on the 8 thermal sensors placed inside the tank at equal distance from each other.

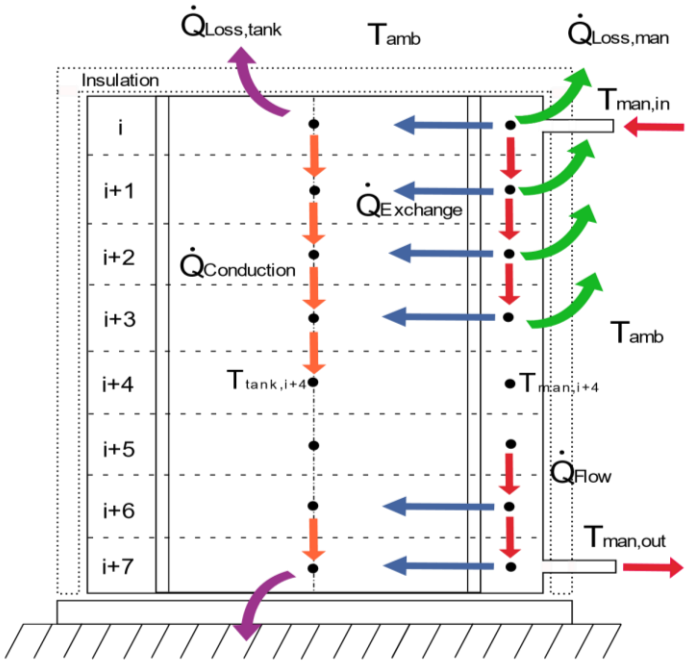

Figure 5. Distribution of the nodes inside the tank and the mantle heat exchanger.

To establish the model equations, we use the following hypotheses [18]:

- In the case of a vertical tank receiving heat at its upper part, the transfer of heat by free convection is considered negligible (Nusselt number equal to one) , and the energy balance equations include only thermal conduction [19];
- The flows exchanged are assumed to be constant over the entire control volume;
- The water flow rate is assumed to be identical throughout the fluid passage section;
- The heat transfer coefficient between the liquid of the mantle on the surface of the heat exchanger is equal to the coefficient of heat transfer from this surface to the liquid in the tank;
- These coefficients are obtained by a linear curve adapted to the experimental data;
- The thermal conductivity, density and specific heat of the glycol water, metal, and insulation are assumed to be constant and independent of temperature;
- The ambient temperature is prescrided as equal on all sides of the module;
- The temperature gradient is assumed to be constant over the distance considered between two nodes.

2.1.7. Mantle Heat Exchanger Stratification

The energy balance for the calculation of the temperature of each node i takes into account the energy of the glycol-water circulating inside the exchanger, the energy transfered to the tank, and the energy lost to the ambient environment. The initial temperature of the heat exchanger preceding the first node (i = 1) is the temperature KT503 (see Figure 3). The energy balance equation is presented in Eq. (17).

$$M_{gw,man,i} c_{p,gw} \cdot \frac{dT_{man,i}}{dt} = \dot{Q}_{Flow,i} - \dot{Q}_{Exchange,i} - \dot{Q}_{Loss,man,i} \tag{17}$$

Substituting the corresponding expression for the the thermal inputs, one gets :

$$M_{gw,man,i} c_{p,gw} \cdot \frac{dT_{man,i}}{dt} = \dot{m}_{gw} c_{p,gw} \left(T_{man,i} - T_{man,i-1}\right) - (U \cdot A)_{man-tank,i} \left(T_{man,i} - T_{tank,i}\right) - \left(\frac{1}{R_{th}}\right)_{man,i} \left(T_{man,mean,i} - T_{amb}\right) \tag{18}$$

The thermal resistance is calculated using the electrical analogy, taking into account the height of the node and the dimensions of the section that surrounds it. The thermal inertia of the heat exchanger is calculated incrementally and the control volume of each node is added to the preceding nodes until the total mass of the exchanger is reached when the fluid arrives at the last node.

2.1.8. Storage Tank Stratification

In a similar way, the calculation of the temperature of node i of the storage tank is obtained via the energy balance equation in Eq. (19). The latter considers the energy transmitted by the mantle heat exchanger to the storage tank and the energy released to the tank. The energy balance equation is expressed in Eq. (19):

$$M_{gw,tank,i} c_{p,gw} \cdot \frac{dT_{tank,i}}{dt} = \dot{Q}_{Exchange,i} + \dot{Q}_{Conduction,i} - \dot{Q}_{Loss,tank,i} \tag{19}$$

Substituting the corresponding expressions for the thermal inputs, one gets :

$$M_{gw,tank,i}c_{p,gw}\cdot\frac{dT_{tank,i}}{dt}=(U\cdot A)_{man-tank,i}\left(T_{man,i}-T_{tank,i}\right)+\left[\left(\frac{1}{R_{th}}\right)_{conduction,i-1}\left(T_{tank,i}-T_{tank,i-1}\right)-\left(\frac{1}{R_{th}}\right)_{conduction,i}\left(T_{tank,i+1}-T_{tank,i}\right)\right]-\left(\frac{1}{R_{th}}\right)_{tank,i}\left(T_{tank,mean,i}-T_{amb}\right) \quad (20)$$

The extraction of the heat exchanger fluid toward the management heat system is located above the last node. The temperatures of the heat exchanger and the tank are adjusted accordingly by reducing the exchange transfer coefficient.

The thermal resistance to conduction between the nodes consists of two parallel resistances. A heat resistance transferred directly through the glycol-water from one node to the other, and a second resistance consisting of two resistances in series: The first resistance corresponds to the resistance between the fluid at the node *i* and the wall of the tank, the second is the resistance of the wall, and the third is the resistance between the wall and the liquid in the next node *i+1*. The resistance can be obtained using Eq. (21). The distance Δx_i considered is calculated between the two nodes.

$$\left(\frac{1}{R_{th}}\right)_{conduction,i}=1/\left(\frac{\Delta x_i}{k_{gw}A_{tank,i}}\right)+1/\left(\frac{1}{h_{gw}\pi\, d_{tank}L_i}+\frac{\Delta x_i}{k_{inox}\pi\, d_{tank}e_{inox}}+\frac{1}{h_{gw}\pi\, d_{tank}L_{i+1}}\right) \quad (21)$$

2.2. Dynamic Simulation

To predict the thermal behavior of each element of the heat management system, the equations presented previously are resolved using Matlab Simulink, a dynamic graphical simulation tool where the subsystems are presented into blocks and connected with each with other thanks to numerical signals in order to ensure the fluid circulation across the heat management system components.

Simulink uses the ode45 solver to solve ordinary differential equations. This solver is based on the Runge-Kutta method with a variable time step. It is one of the most commonly used methods in solving mathematical models for mechanical engineering, thermal, electrical applications. The maximum relative error (set to $1\cdot10^{-4}$ by default) as well as other parameters of the solver, such as the maximum and minimum size of the time step, can be modified by the user or automatically optimized by the simulation tool.

Figure 6 shows the structure of the model implemented in Simulink. The inlet parameters are on the upper left part of the figure while the control flow chart is on the upper right part of the figure. The simulation data is presented in Table 2, and the data that was collected is derived from the constructor manual [10, 20] and different catalogues that are available online [21- 25].

The selected mode for the simulation is cooling with storage combined with the dry cooler. The resulting temperatures are displayed during the simulation and sent to the Matlab workspace for errors calculation and simulation accuracy. The control and monitoring of the system are fulfilled by using a flow chart diagram.

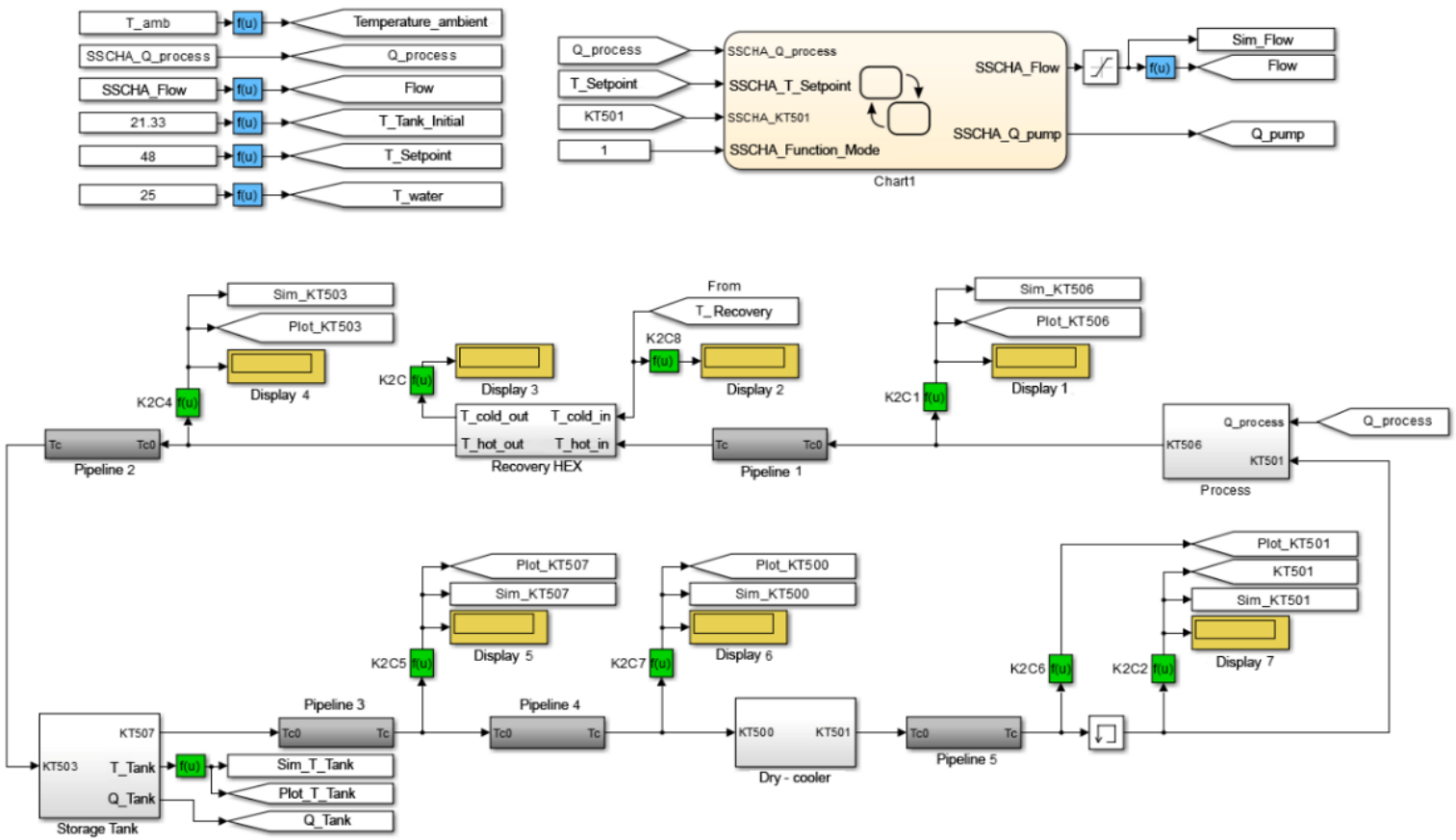

Figure 6. Screenshot of the heat management system numerical simulation.

Table 2. Heat management system simulation parameters

Glycol-water			Recovery heat exchanger		
h_{gw}	100-900 W m^{-2} K^{-1}	[22]	V_{plates}	$40 \cdot 10^{-3}$ m^3	[10]
ρ_{gw}	1025 kg m^{-3}	[21]	V_{shell}	$5 \cdot 10^{-3}$ m^3	[10]
$c_{p,gw}$	3.61 J kg^{-1} K^{-1}	[22]	R_{shell}	$136 \cdot 10^{-3}$m	[10]
Stainless steel			L_{shell}	$86 \cdot 10^{-2}$ m	[10]
k_{inox}	16.3 W m^{-1} K^{-1}	[23]	A_{hex}	1.90 m^2	[10]
ρ_{inox}	7900 kg m^{-3}	[23]	M_{hex}	75 kg	[10]
$c_{p,inox}$	502 J kg^{-1} K^{-1}	[23]	Dry cooler		
ε_{inox}	$3 \cdot 10^{-3}$ m	[21]	L_{cooler}	504 m	[10]
Insulation material			d_{cooler}	10^{-2} m	[10]
ρ_{insul}	20 kg m^{-3}	[24]	M_{cooler}	1150 kg	[10]
k_{insul}	0.036 W m^{-1} K^{-1}	[24]	Pipeline diameter		
$c_{p,insul}$	1300 J kg^{-1} K^{-1}	[24]	d_1	$\cdot 10^{-3}$ m	[10]
ε_{insul}	$50 \cdot 10^{-3}$ m	[21]	d_2	$50 \cdot 10^{-3}$ m	[10]
Air			d_3	$140 \cdot 10^{-3}$ m	[10]
h_{air}	5-25 W m^{-2} K^{-1}	[25]	Pump		
k_{air}	0.025 W m^{-1} K^{-1}	[25]	$\dot{W}_{electric}$	1.85 kW	[10]
Tank & Mantle heat exchanger			η_{pump}	63 %	[10]
M_{tank}	2100 kg	[10]	Fuel cell [20]		
V_{man}	$75 \cdot 10^{-3}$ m^3	[10]	$\eta_{Fuel\ Cell}$	47%	[20]
V_{tank}	15 m^3	[10]	$\dot{Q}_{process}$	100 kW	[20]
L_{tank}	4 m	[10]			
d_{tank}	2.2 m	[10]			
$A_{man-tank}$	25 m^2	[10]			

Regarding the glycol-water mass flow rate $\dot{m}_{gw}$, its value is proportional to the temperature of the fluid returning to the process heat exchanger, also known as the outlet temperature of the dry cooler. A linear regression is performed based on the experimental measures of the temperature $T_{cooler,out}$ and the fluid volume flow rate. The equation obtained is displayed in Figure 7.

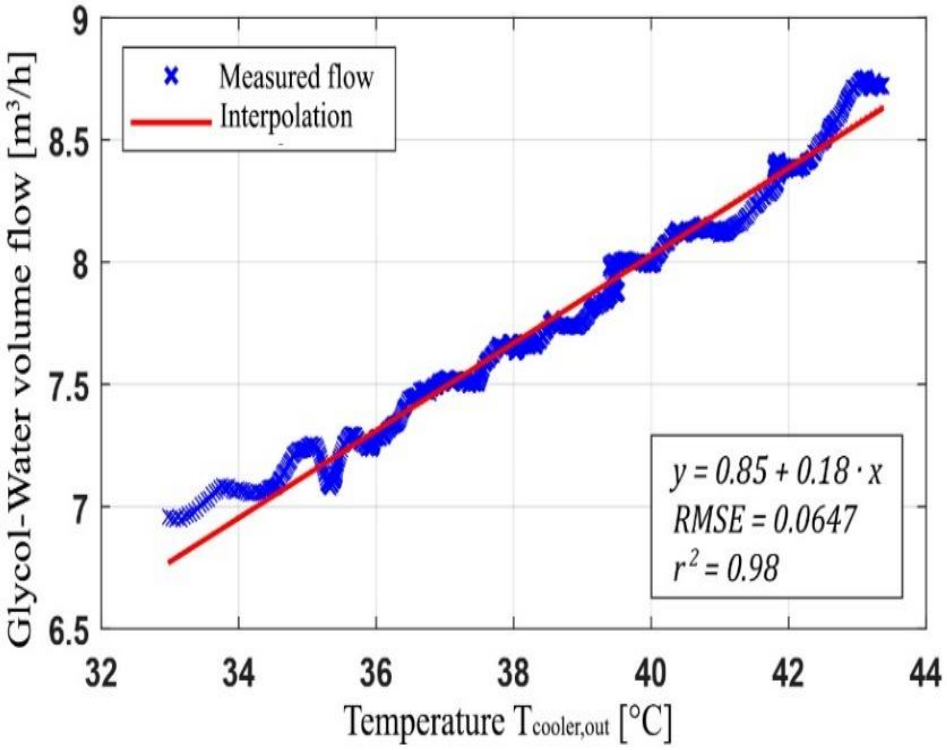

Figure 7. Linear correlation between the volume flow rate of the glycol-water and the outlet temperature of the dry cooler.

2.3. Experimental Validation

Figure 8 presents a first experiment performed on 23/06/2016 to estimate the thermal storage capacity of the tank. The fuel cell is turned on from 9 a.m. to 10 p.m. (13 continuous hours) at a nominal thermal power of 100 kW and a cooling set point temperature of 50 °C. During the experiment, an alarm went off, which puts the fuel cell in stand-by mode at around 12:20 p.m. (hence the peak down). Later, the fuel cell was restarted manually.

Figure 9 presents the temperatures measured by the heat sensors (KT). The disturbances noise is due to the sensitivity of the PID controller that governs the circulation pump of the process. The temperature of the storage tank is averaged from the measures of the 8 heat sensors placed vertically inside the tank.

A second experiment was performed the next day to investigate the thermal discharge of the storage tank. The MYRTE platform was shut down and the heat management system was manually insulated from the rest of the platform. The system temperature changes depend mainly on the ambient temperature.

An adjustment of the calculated thermal inertia, the thermal resistance and the outward loss values was necessary. This procedure was carried out using an optimization tool and the results are shown in Table 3.

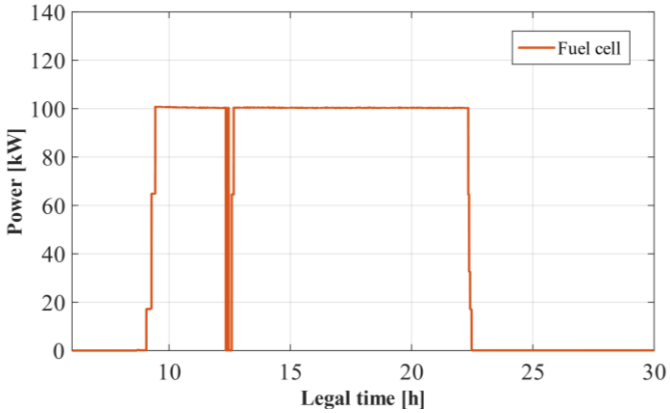

Figure 8. Electric power of the fuel cell.

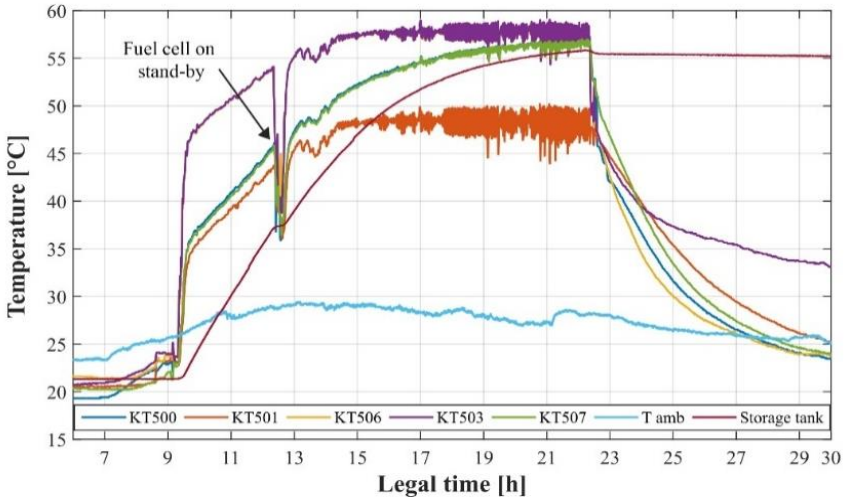

Figure 9. Heat management system experimental temperatures.

Table 3. Experimentally refined parameters

Parameter	Calculated value	Refined value
$(U \cdot A)_{man\text{-}tank}$	6506 W K^{-1}	6637.5 W K^{-1}
$(U \cdot A)_{cooler}$	1300 W K^{-1}	1392 W K^{-1}
$(U \cdot A)_{man}$	$9.9 \cdot 10^{-4}$ W K^{-1}	$18.6 \cdot 10^{-4}$ W K^{-1}
$(M \cdot c_p)_{tank}$	$58.9 \cdot 10^{6}$ J K^{-1}	$64.8 \cdot 10^{6}$ J K^{-1}
$(M \cdot C_p)_{cooler}$	$45.4 \cdot 10^{5}$ J K^{-1}	-

In order to estimate the power of each element of the heat management system, the following equations are used [20].

Recovery heat exchanger power

$$\dot{Q}_{recovery} = \dot{m}_{gw} \cdot c_{p,gw} \cdot (T_{shell,in} - T_{shell,out}) \quad (22)$$

Dry cooler's power

$$\dot{Q}_{dry\ cooler} = \dot{m}_{gw} \cdot c_{p,gw} \cdot (T_{cooler,in} - T_{cooler,out}) \quad (23)$$

Storages capacity

$$\dot{Q}_{tank} = \dot{m}_{gw} \cdot c_{p,gw} \cdot (T_{man,in} - T_{man,out}) \quad (24)$$

3. Results and Discussion

3.1. Temperatures and Volumetric Flow Rate

To evaluate the agreement between the experimental and calculated parameters, the MAE and nRMSE indicators are used. The simulated profiles are smooth compared to the measured parameters as the PID fluctuations are not considered. Also, the shutdown of the system at 12:00 p.m. is not taken into account. In Figure 10 a good agreement between the simulated and measured temperatures is observed, as the nRMSE calculation varies from 0.48 to 2.29%. Regarding the storage tank mean temperature in Figure 10.f, a MAE deviation of 0.40°C confirms the validity of the assumptions made for the calculation of this temperature. Furthermore, a good agreement with the experimental data is observed for the volumetric flow rate with a normalized error of 0.71% as shown in Figure 11.

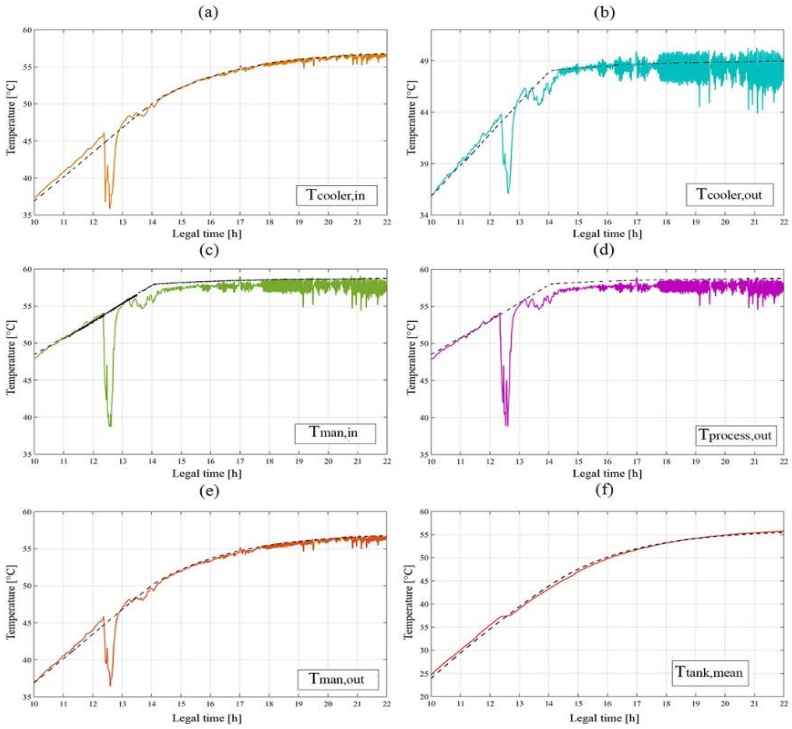

Figure 10. The simulated (doted lines) and measured (continuous lines) fluid tempertaures.

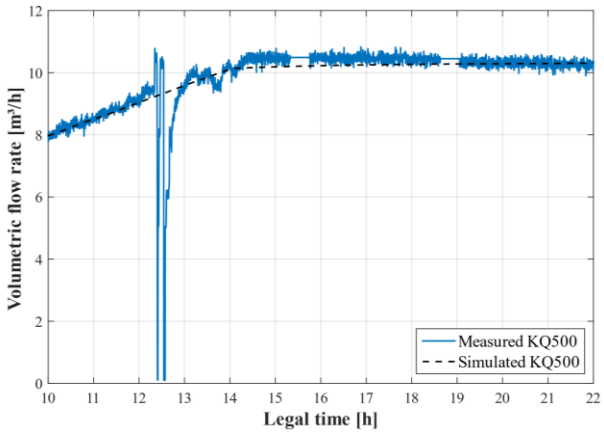

Figure 11. The volumetric flow rate of the glycol-water.

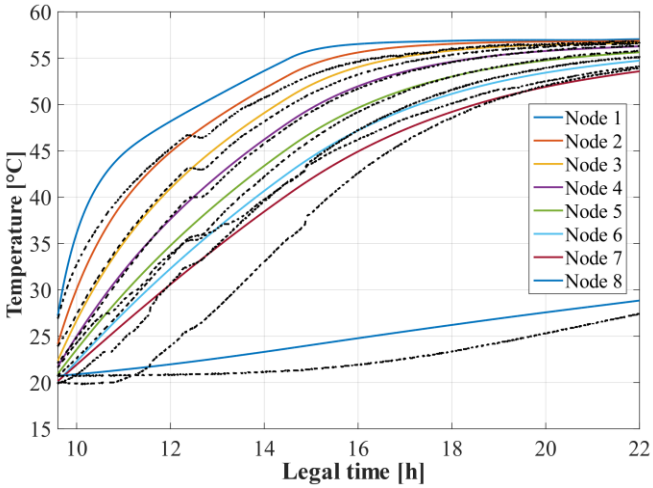

Figure 12. Measured and simulated temperatures of the nodes inside the tank.

Figure 12 shows the thermal stratification inside the storage tank. The simulated temperature of the nodes (continuous lines) is higher than the measured one (dotted lines). The simulation data is overestimating the temperature, this is due to the simplifying hypothesis considered in the stratification model, as for instance the constancy of the temperature inside the control volume. This results into a stronger heat exchange for the simulation.

When it comes to the temperature of the fluid leaving the heat exchanger (node 8), modeling with the average temperatures gives better results (Method 1) than with the stratified model (Method 2), as shown in Figure 13. A maximum gap of 2°C is more likely due to the simplifying calculation assumptions cited previously. The control volume choice may also have its influence as the first method takes into consideration the mean temperature of the metal and insulation along with the fluid. The obtained temperatures from the two simulations methods (stratified and mean temperature) are then compared. The MAE and nRMSE are found to be 2.26°C and 6%, respectively.

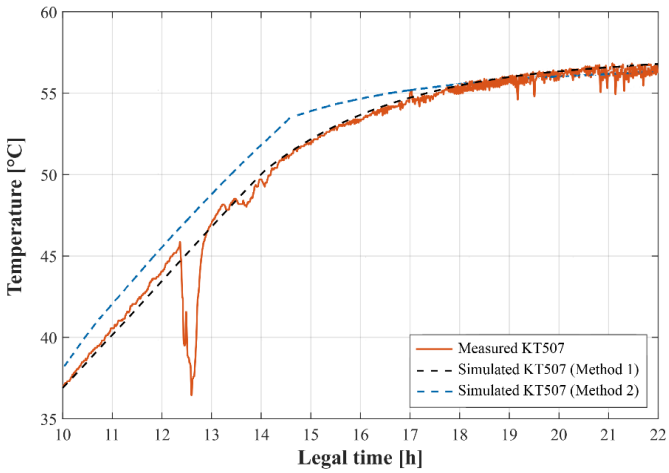

Figure 13. Temperature at the outlet of the mantle heat exchanger.

The next weeks following this experiment, the heat management system was shut down. The tank temperature became uniform in the upper half of the tank (Figure 14), and the maximum temperature decreased by 1°C every three days. This experiment allows to estimate the storage tank and mantle heat exchanger loss to the outside.

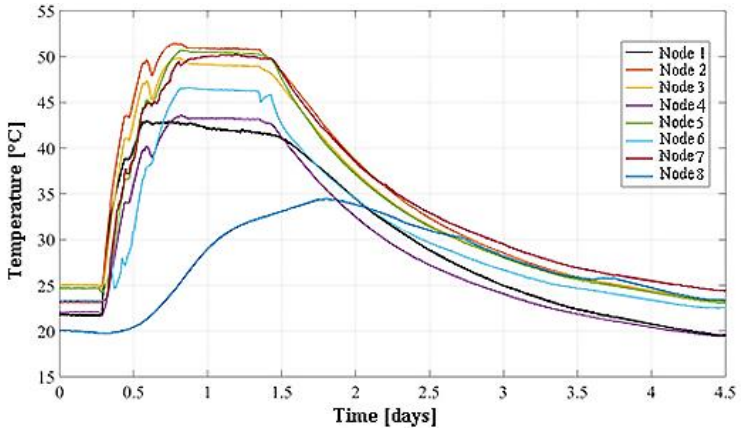

Figure 14. Experimental temperatures profile inside the storage tank.

3.2. Powers

Figure 15 compare measured (full lines) and simulated (dashed lines) powers of the heat management system. To simplify the energy balance equation, the system is divided into three parts : The global heat flow of the process is a combination of heat stored in the tank ($\dot{Q}_{tank}$), dissipated within the pipelines ($\dot{Q}_{auxillary}$) or through the dry cooler ($\dot{Q}_{drycooler}$).

$$\dot{Q}_{process} = \dot{Q}_{tank} + \dot{Q}_{auxilary} + \dot{Q}_{drycooler} \tag{27}$$

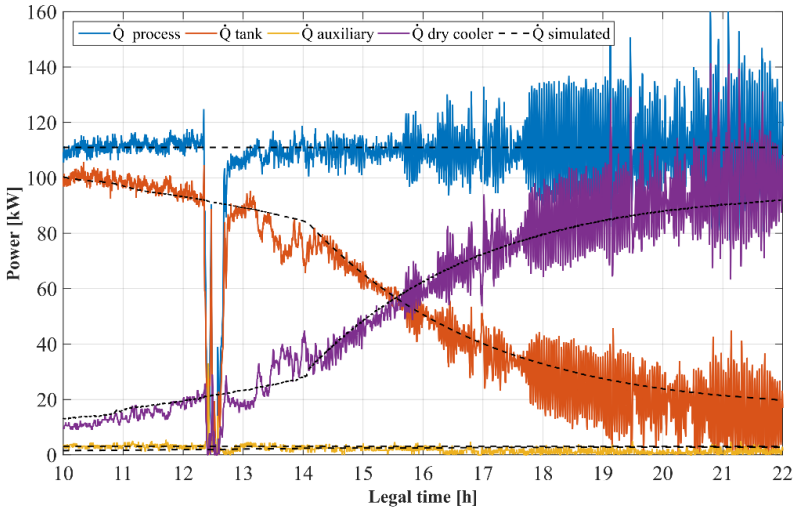

Figure 15. Evolution of the simulated and measured power.

By analyzing the experimental curve of the tank and the dry cooler, it can be seen that once the tank is full (at 13h), $\dot{Q}_{tank}$ decreases rapidly. At this point, the tank is not able to store more heat than it receives when it reaches the inlet temperature of the mantle heat exchanger, it is then a wasted energy as it is dissipated throughout the dry cooler. For this reason, it is interesting to consider an operation mode of the fuel cell with heat storage combined with recovery, which makes use as little as possible of the dry cooler.

CONCLUSION

The majority of hydrogen chains coupled with renewable energy sources focus on electrical production unlike the MYRTE platform that benefits from a heat management system designed for cooling the electrolyzer and fuel cell units, and that tries to value the heat produced by both units.

The aim of the present study is to establish a model capable of describing the operation of the heat management system of the MYRTE platform in a conventional cooling mode with storage of the heat throughout the mantle heat exchanger in order to be able to use the produced heat for recovery and cogeneration. The system is modeled via energy balance equations which are based on a lumped parameter model to calculate the subsystem temperatures, and the first order differential equations obtained are solved using Matlab Simulink.

The proposed model describes the behavior of the different elements composing the cooling process with an average nRMSE of 1.38% and 0.71% for the temperatures and the volumetric flow rate, respectively. The simulated powers of the process, the tank, the dry cooler and the auxiliaries are consistent with the measured platform data.

The investigation has shown that the storage tank is well stratified and can be further optimized to enhance its storage capacity. This can be achieved by lowering the extracting point of the heat exchanger fluid.

The dry cooler is the most energy consuming device in the heat management system. New operation strategies can be considered to enhance the system by recovering the heat produced for heating or cooling purposes.

Further studies will be carried out to investigate numerically the discharge of the recovery mode of the heat management system through an association with a solar adsorption chiller.

ACKNOWLEDGMENTS

MYRTE project is a supported by AREVA Energy Storage, the CEA, the European Union, the French government and the Corsican territorial collectivity.

ETHICAL COMPLIANCE

MYRTE project is a supported by AREVA Energy Storage, the CEA, the European Union, the French government and the Corsican territorial collectivity. The authors declare that they have no conflict of interest.

REFERENCES

[1] International Energy Agency IEA, *"Key World Energy Statistics,"* 2016.

[2] D. S. Kim and C. A. Infante Ferreira, "Solar refrigeration options - a state-of-the-art review," *International Journal of Refrigeration*, vol. 31, no. 1, pp. 3–15, Jan. 2008.

[3] Intergovernmental Panel on Climate Change (IPCC), *UN Climate Change 2014*, 2014.

[4] SudOuest.fr, *Climat : l'UE signe un accord historique contre les gaz à effet de serre* [*Climate: EU signs landmark agreement on greenhouse gases*], 2014. [Online]. Available: http://www.sudouest.fr/2014/10/24/climat-l-ue-signe-un-accord-historique-contre-les-gaz-a-effet-de-serre-1714937-706.php. [Accessed: 04-Feb-2015].

[5] UNFCCC, "Paris Agreement," *Conference of the Parties on its twenty-first session*, vol. 21932, no. December, p. 32, 2015.

[6] Florides, S. . Tassou, S. . Kalogirou, and L. . Wrobel, "Review of solar and low energy cooling technologies for buildings," *Renewable and Sustainable Energy Reviews*, vol. 6, no. 6, pp. 557–572, Dec. 2002.

[7] Z. Hassan and A. A. Mohamad, "A review on solar-powered closed physisorption cooling systems," *Renewable and Sustainable Energy Reviews*, vol. 16, no. 5, pp. 2516–2538, Jun. 2012.

[8] H. Z. Hassan, A. A. Mohamad, and H. A. Al-Ansary, "Development of a continuously operating solar-driven adsorption cooling system: Thermodynamic analysis and parametric study," *Applied Thermal Engineering*, vol. 48, pp. 332–341, Dec. 2012.

[9] G. Mariano and D. Petit, *La plate-forme {B}{C}aml* [*The platform {B} {C} aml*] 2002. [Online]. Available: http://myrte.univ-corse.fr/La-plateforme_a4.html. [Accessed: 15-Jan-2015].

[10] Areva SE, *Spécification Technique de Besoin pour un système de gestion de la chaleur dans une chaine d'hydrogène*, [*Technical Requirement Specification for a Heat Management System in a Hydrogen Chain*] France, 2008.

[11] M. Espinosa-López et al., "Modelling and experimental validation of a 46 kW PEM high pressure water electrolyzer," *Renewable Energy*, vol. 119, pp. 160–173, Apr. 2018.

[12] C. Darras, M. Muselli, P. Poggi, C. Voyant, J.-C. Hoguet, and F. Montignac, "PV output power fluctuations smoothing: The MYRTE platform experience," *International Journal of Hydrogen Energy*, vol. 37, no. 19, pp. 14015–14025, Oct. 2012.

[13] C. DARRAS, *Modélisation de systèmes hybrides Photovoltaïque / Hydrogène : Applications site isolé, micro-réseau, et connexion au réseau électrique dans le cadre du projet PEPITE (ANR PAN-H)* [*Hybrid Photovoltaic / Hydrogen Systems Modeling: Isolated Site Applications, Micro-Grid, and Connection to the Power Grid as part of the PEPITE Project (ANR PAN-H)*] France, 2010.

[14] Rodler, P. Haurant, G. Faggianelli, G. Pigelet, and P. Poggi, "Combined heat and power generation of the hydrogen chain based on MYRTE platform," *International Solar Energy Society*, no. November, pp. 8–12, 2015.

[15] S. A. Klein, W. A. Beckman, J. W. Mitchell, and J. A. Duffie, *Mathematical ReferenceTranNsient System Simulation Programm*, 2014.

[16] Huang, S. Pu, W. Gao, and Y. Que, "Experimental investigation on thermal performance of thermosyphon flat-plate solar water heater with a mantle heat exchanger," *Energy*, vol. 35, no. 9, pp. 3563–3568, Sep. 2010.

[17] Y. M. Han, R. Z. Wang, and Y. J. Dai, "Thermal stratification within the water tank," *Renewable and Sustainable Energy Reviews*, vol. 13, no. 5, pp. 1014–1026, 2009.

[18] P. Berg and S. Furbo, "Calculation of the thermal performance of small hot water solar heating systems using low flow operation." In: *Energy Conservation in Buildings*, 1991, pp. 357–362.

[19] M. A. B. Yunus A. Cengel, Y. A. Cengel, and M. A. Boles, "Thermodynamics: an engineering approach." In: *Sea*, vol. 1000, 2002, p. 8862.

[20] Thermi-Consult and Groupe Ziemann, *Heat Management System Exploitation File*, 2006.

[21] S. Khattab, F. Bandarkar, M. Khoubnasabjafari, and A. Jouyban, "Density, viscosity, surface tension, and molar volume of propylene glycol + water mixtures from 293 to 323 K and correlations by the Jouyban–Acree model," *Arabian Journal of Chemistry*.

[22] Dow, "A Guide To Glycols," *A guide to Good Research Practice*. pp. 1–35, 2003.

[23] S. D. D. du D. technologique D. de l'Évaluation et de la Sensibilisation [DDA D. Technological D D. Evaluation and Awareness], *Fiche matériaux Métaux, l' Inox, Acier inoxydable*. p. 2, 2010.

[24] Daniel WYART, *Polystyrène expansé ou PSE - Propriétés du polystyrène expansé*, [*Expanded polystyrene or EPS - Properties of expanded polystyrene*] 2008. [Online]. Available: https://www.techniques-ingenieur.fr/base-documentaire/materiaux-th11/matieres-thermoplastiques-monographies-42147210/polystyrene-expanse-ou-pse-am3341/proprietes-du-polystyrene-expanse-am3341niv10004.html. [Accessed: 20-Dec-2015].

[25] The Engineering Tool Box, *Dry Air Properties*. [Online]. Available: https://www.engineeringtoolbox.com/dry-air-properties-d_973.html. [Accessed: 20-Dec-2017].

[26] G. Notton, *State of the art forecasting tools Photovoltaic production forecasting in literature*, Ajaccio, 2016.
[27] COST, *Weather Intelligence for Renewable Energies (WIRE)*, ES1002, 2012.